# RSC Advances

Journal Name

Dynamic Article Links ▶

## ARTICLE TYPE

# Simultaneously improving the thermal stability, flame retardancy and mechanical properties of polyethylene by the combination of graphene with carbon black

Jiang Gong,[a,b] Ran Niu,[a,b] Jie Liu,[a] Xuecheng Chen,[a,c] Xin Wen,[a] Ewa Mijowska,[c] Zhaoyan Sun[a]
5 and Tao Tang*[a]

A novel combination of graphene nanosheet (GNS) with carbon black (CB) was demonstrated to significantly improve the thermal stability, flame retardancy and mechanical properties of linear low
10 density polyethylene (LLDPE). The temperature at the maximum weight loss rate of LLDPE under air flow was dramatically increased by 94.3 °C, and the peak value of heat release rate of LLDPE nanocomposite measured by cone calorimeter was obviously reduced from 1466 to 297 kW/m$^2$ (by 80%). According to the results from rheological tests and structural characterization of residual chars, the improved thermal stability and flame retardancy of LLDPE were partially attributed to the formation of a
15 percolated network structure by GNS and CB in LLDPE matrix, and partially to the accelerated oxidation crosslinking reaction of LLDPE radicals catalyzed by CB and GNS. More importantly, although both GNS and CB were commercial and used without any pre-treatments, LLDPE nanocomposites incorporating both the nanofillers showed much higher mechanical properties compared to neat LLDPE, especially Young's moduli which was improved by 219%. This was ascribed to good dispersions of two
20 nanofillers and strong matrix-nanofiller interfacial interactions.

## 1. Introduction

The addition of nanofillers into polymer matrix has been demonstrated to remarkably improve the physical and chemical properties such as mechanical properties and flame retardancy of
25 polymer matrix.[1–4] According to nanofiller shape, the most commonly used nanofillers for polymer nanocomposites can be classified as follows: layered (two-dimension) such as clay[5–10] and graphene,[11,12] fiber-like (one-dimension) such as carbon nanotubes (CNTs),[13–16] and spherical (zero-dimension) such as
30 C60[17] and carbon black (CB),[18] etc. With the research for the utility of different nanofillers in nanocomposites and the demand for high-performance composites, the combination of different nanofillers to prepare multifunctional polymer nanocomposites has been believed to be a more attractive strategy.[19–26] This is
35 because nanofillers with different geometrical dimensions could present a synergistic effect on enhancing the flame retardancy and other properties of polymer matrix.

For example, Ma et al. founded that the combination of CNTs with clay significantly improved the flame retardancy of
40 acrylonitrile-butadiene-styrene resin, in which the mechanism was attributed to the formation of a network structure of CNTs and clay.[27] Song et al. reported the improvement of flame retardancy and mechanical properties of polypropylene (PP) by C60-decorated CNTs due to the free-radical trapping effect of
45 C60 and the network of CNTs.[28] Liu et al. prepared ternary

polyurethane/graphene nanoribbon/CNT nanocomposite with excellent mechanical properties and high electrical conductivity.[29] Recently, our group successfully prepared many multicomponent polymer nanocomposites containing nickel nanoparticles and
50 reactive nanofillers such as chlorinated CNTs.[30–38] A large amount of chars including CNTs were in situ formed from the carbonization of degradation products of polymer itself under the combined catalysis of nickel nanoparticles and reactive nanofillers in the intermediate stage of combustion. In this case,
55 the amount of evolved flammable volatiles was reduced, and the flame retardancy of the polymer was thus improved. Meanwhile, the reactive nanofillers could improve the mechanical properties of polymer matrix at room temperature.[35]

However, although many investigations have been carried on
60 to study the combination of nanofillers with different geometrical dimensions on improving the flame retardancy and other properties of polymer matrix, little attention has been paid to the combination of two-dimensional nanofiller with zero-dimensional nanofiller on improving the performances of polymer matrix, for
65 example, graphene and CB. Compared to other nanofillers, graphene has received significant attention for its high surface area, aspect ratio, fascinating electrical, mechanical, thermal and chemical properties since 2004.[39] As we know, CB is fabricated from fuel-rich partial combustion and has been used for ink,
70 pigments and tattoos for more than 3000 years.[40] The total production of CB was up to 8,100,000 metric tons in 2006.[41] Previous work has demonstrated that CB can not only delay the

heat transport from flame into polymer matrix, leading to a slower increase of temperature in the polymer matrix,[11] but also trap peroxy radicals of polymer at elevated temperature to form a gelled-ball crosslinking network, and thus remarkably improve the flame retardancy of polymer.[18, 42, 43] However, to the best of our knowledge, the effect of the combination of graphene with CB on the thermal stability, flame retardancy and mechanical properties of polymer has not yet been studied.

Herein, the combination of graphene nanosheet (GNS) with CB was demonstrated to notably improve thermal stability, flame retardancy and mechanical properties of linear low density polyethylene (LLDPE). Our attention was focused on the influences of the mesoscopic network of GNS with CB and the oxidation crosslinking reaction of LLDPE radicals catalyzed by CB and GNS on the thermal stability and flammability of LLDPE. More importantly, it is very attractive to prepare multicomponent polymer nanocomposites showing significant improvements in thermal stability and flame retardancy without compromising other performances such as mechanical properties.

## 2. Experiment part

### 2.1 Materials

Linear low density polyethylene (LLDPE, trademark DFDA-7042, weight–average molecular weight index $1.41 \times 10^5$ g/mol, and polydispersity index 3.36) powder was supplied by Sinopec Maoming Company. GNS (code KNG-G5, thickness < 5 nm, size 0.1–5 μm, and purity > 99 %) was obtained from Xiamen Knano Graphene Technology Co., Ltd., Xiamen, China. CB (purity > 99%) was purchased from Linzi Qishun Chemical Co., Shandong, China, with the original particle diameter of 17 nm.

### 2.2 Preparation of LLDPE nanocomposites

LLDPE nanocomposites were prepared by mixing LLDPE powder with GNS and/or CB in a Haake batch intensive mixer (Haake Rheomix 600, Karlsruhe, Germany) at 100 rpm and 160 °C for 10 min. The resultant samples were designated as xGNSyCB. Here x and y denote the weight percentages of GNS and CB, respectively. For example, 3GNS5CB means that the LLDPE nanocomposite contains 3 wt % GNS and 5 wt % CB.

### 2.3 Characterization

The dispersion states of GNS and CB in LLDPE matrix were examined with field-emission scanning electron microscope (FE-SEM, XL30 ESEM-FEG, FEI Co.). The samples were fractured in liquid nitrogen, and the fracture surfaces were coated with gold before FE-SEM observation. Thermal gravimetric analysis (TGA) was performed on a SDTQ600 thermal analyzer (TA Instruments). The samples for LLDPE and its nanocomposites with mass of 7.5 ± 0.2 mg were heated from room temperature at 10 °C/min under air atmosphere. Cone calorimeter tests were performed using a Fire Testing Technology Ltd. (West Sussex, UK) device according to ISO 5660 at an incident flux of 50 kW/m², and the size of specimens was 100 mm × 100 mm × 6.0 mm. The photographs of the residual chars after the cone calorimeter tests were collected by a digital camera. The interior structure of the residual chars was further examined by FE-SEM (XL30 ESEM-FEG). The limiting oxygen index (LOI) values were measured on an HC-2C oxygen index meter (Jingning Analysis Instrument Company, China) with sheet dimensions of 130 mm × 6.5 mm × 3.2 mm according to ISO4589-1999. The vertical burning tests were conducted according to the UL-94 test standard (ASTM D 3801) with the test specimen of 130 mm × 13 mm × 3 mm. The rheological measurements of LLDPE and its nanocomposites were carried out on a controlled strain rate rheometer (ARES rheometer). The size of samples measured was 25 mm in diameter, with a gap of 1.0 mm. Frequency sweeping was performed at 160 °C at a frequency from 0.01 to 100 rad/s in nitrogen environment, with a strain of 1% in order to make the materials be in the linear viscosity range. Temperature scanning test was performed in the range from 160 to 400 °C after samples were preheated at 160 °C for 10 min, with a strain of 1% and a fixed frequency of 0.1 rad/s in air environment. Mechanical properties were measured on an Instron 1121 at an extension speed of 20 mm/min. The specimens were prepared by mold pressing at 160 °C with the size of (70 mm × 40 mm × 1 mm) rectangle plaques and cut into dumbbell specimens with the middle part size of 20 mm × 4 mm × 1 mm. All data were the average of five independent measurements; the relative errors committed on each data were reported as well.

## 3. Results and discussion

### 3.1 Dispersion states of GNS and CB in LLDPE matrix
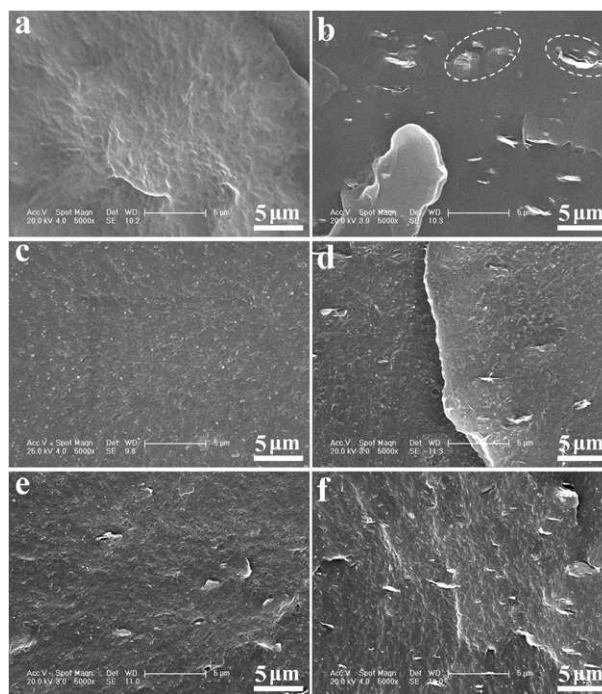


**Fig. 1** Typical FE-SEM images of the brittle-fractured surfaces of LLDPE and its nanocomposites: (a) neat LLDPE, (b) 3GNS, (c) 5CB, (d) 1GNS3CB, (e) 1GNS5CB and (f) 3GNS5CB.

The dispersion of nanofillers in polymer matrix and the interfacial interaction between polymer matrix and nanofillers are two most important factors influencing the properties of polymer nanocomposites. The dispersion states of GNS and CB in LLDPE matrix are shown in Fig. 1. It was apparent that GNS was uniformly distributed in the binary 3GNS nanocomposite with the size in the range of 0.1–5 μm (Figs. 1a and 1b), and some GNS

aggregates were also observed (marked by dashed line in Fig. 1b). As shown in Fig. 1c, CB nanoparticles were well dispersed in the binary 5CB nanocomposite with the diameter in the range of 60–100 nm. Furthermore, it was found that the addition of CB into
5 binary 3GNS nanocomposite promoted the dispersion of GNS in the LLDPE matrix (Figs. 1d–1f). There are two possible reasons for the above phenomena. One of them results from the viscosity increase of the matrix due to the fast dispersion of a nanofiller, which increases shear force during melt mixing and improves the
10 dispersion degree of the other nanofiller. The other is possible interaction between the two nanofillers, which prevents re-aggregation of the dispersed nanofillers. As a result, GNS and CB were well dispersed in the ternary LLDPE nanocomposites.

15 **3.2 Thermal stability**



**a**

**b**
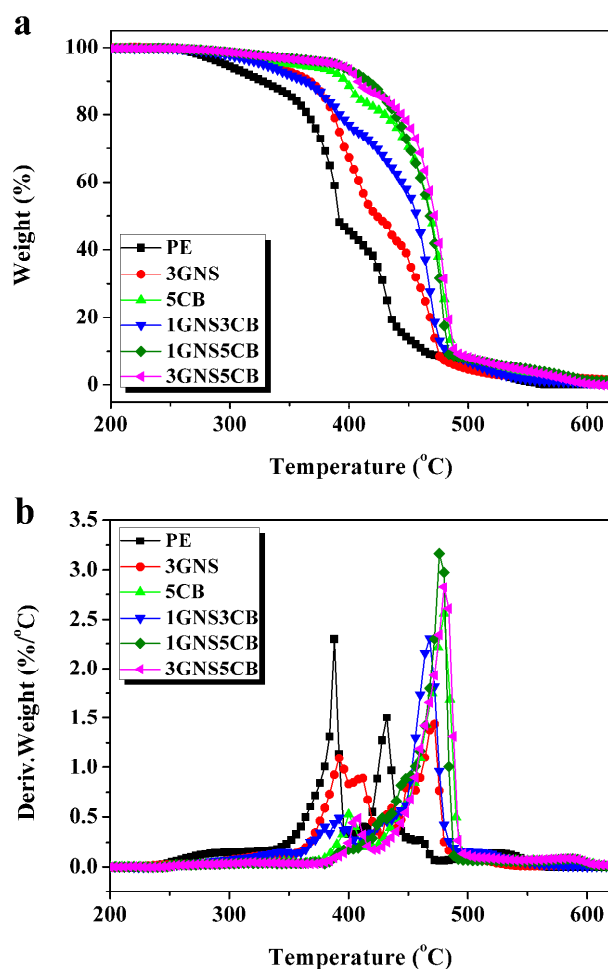
**Fig. 2** TGA (a) and DTG (b) curves of LLDPE and its nanocomposites under air atmosphere at 10 °C/min.

20 To study the influences of GNS and CB on the thermal stability of LLDPE, TGA measurements were conducted. Fig. 2 presents TGA and DTG (the first derivative of TGA curve) curves for LLDPE and its nanocomposites under air atmosphere at 10 °C/min. $T_{5wt\%}$, $T_{10wt\%}$, $T_{50wt\%}$ and $T_{max}$ represented the temperature
25 at which 5 wt %, 10 wt %, 50 wt % and the maximum weight loss rate occurred, respectively. Detailed data are listed in Table 1. For

neat LLDPE, the first peak in DTG curve was probably attributed to the oxidation degradation of short branches, while the second peak was mainly owing to the oxidation decomposition of the
30 crosslinking structure.[44] Evidently, the thermal stability of LLDPE nanocomposites increased compared with those of neat LLDPE. In the case of binary 3GNS nanocomposite, $T_{5wt\%}$, $T_{10wt\%}$, $T_{50wt\%}$ and $T_{max}$ were obviously increased by 36.1, 39.6, 34.1 and 83.1 °C, respectively, compared to neat LLDPE. Comparatively,
35 $T_{5wt\%}$, $T_{10wt\%}$, $T_{50wt\%}$ and $T_{max}$ of binary 5CB nanocomposite were remarkably increased by 56.3, 69.8, 79.2 and 92.0 °C, respectively. Interestingly, the combination of GNS with CB further enhanced the thermal stability of LLDPE. In particular, for ternary 3GNS5CB nanocomposite, $T_{5wt\%}$, $T_{10wt\%}$, $T_{50wt\%}$ and
40 $T_{max}$ were 93.0, 80.5, 82.7 and 94.3 °C higher than those of neat LLDPE, respectively. Accordingly, the combination of GNS with CB was more efficient than GNS or CB alone in enhancing the thermal stability of LLDPE. The main reason was probably ascribed to more efficiently trapping LLDPE radicals to form
45 branched macromolecules by CB nanoparticles,[18,43] when GNS was simultaneously added.

**Table 1** Summary of the TGA results (Fig. 2) for LLDPE and its nanocomposites under air atmosphere.

| Sample | $T_{5wt\%}$ [a] (°C) | $T_{10wt\%}$ [b] (°C) | $T_{50wt\%}$ [c] (°C) | $T_{max}$ [d] (°C) |
|---|---|---|---|---|
| PE | 295.3 | 327.4 | 389.4 | 387.4 |
| 3GNS | 331.4 | 367.0 | 423.5 | 470.5 |
| 5CB | 351.6 | 397.2 | 468.6 | 479.4 |
| 1GNS3CB | 327.6 | 363.0 | 456.6 | 467.0 |
| 1GNS5CB | 389.5 | 415.9 | 468.0 | 477.7 |
| 3GNS5CB | 388.3 | 407.9 | 472.1 | 481.7 |

50 [a] $T_{5wt\%}$ represented the temperature at which 5 wt % weight loss occurred. [b] $T_{10wt\%}$ represented the temperature at which 10 wt % weight loss occurred. [c] $T_{50wt\%}$ represented the temperature at which 50 wt % weight loss occurred. [d] $T_{max}$ represented the temperature at which the maximum weight loss rate occurred.

55
**3.3 Flammability properties**
The influences of GNS and CB on the flame retardancy of LLDPE were investigated by means of cone calorimetry. Cone calorimetry is one of the most effective small-sized polymer fire
60 behavior tests. It provides some important parameters such as the time to ignition ($t_i$), heat release rate (HRR), peak heat release rate (PHRR), the total heat release (THR) and the mass loss rate (MLR), etc. Fig. 3 shows the HRR plots of LLDPE and its nanocomposites measured by cone calorimeter at 50 kW/m². It
65 was observed that neat LLDPE burnt very fast after ignition and a sharp HRR peak appeared with a PHRR as high as 1466 kW/m². The PHRR in the HRR plot of binary nanocomposites (3GNS and 5CB) were 670 and 320 kW/m², which were reduced by 54% and 79%, respectively, compared to that of neat LLDPE. This result
70 indicated that the flammability of LLDPE was influenced to an extent by adding GNS or CB alone. The lower $t_i$ values of binary

nanocomposites compared to neat LLDPE (Table 2) were probably attributed to the catalytic effect of GNS or CB on the degradation of LLDPE. When the combination of GNS and CB was applied, the PHRR from the HRR plots of ternary LLDPE/GNS/CB nanocomposites showed a further reduction. Typically, the HRR plot of ternary 3GNS5CB nanocomposite showed the lowest peak value (PHRR = 297 kW/m$^2$) and reduced further after the peak, and stayed at a very low level throughout. Similar with binary 5CB nanocomposite, LLDPE/GNS/CB nanocomposites showed lower $t_i$ values than neat LLDPE.
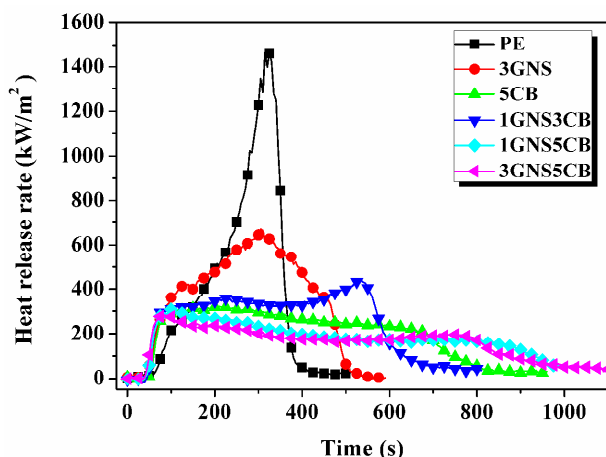


**Fig. 3** Effect of GNS and CB on the heat release rate of LLDPE at an incident heat flux of 50 kW/m$^2$.
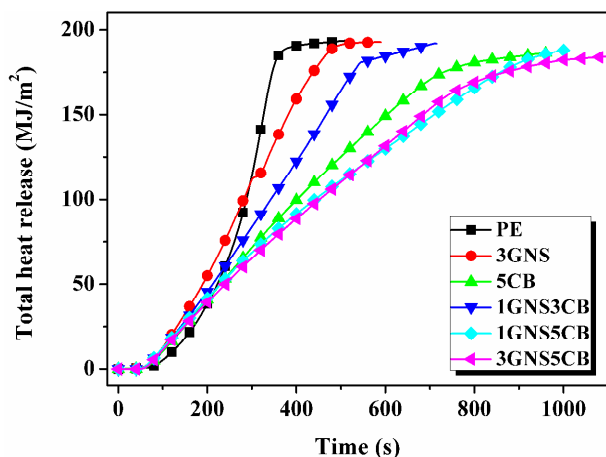


**Fig. 4** Effect of GNS and CB on the total heat release of LLDPE.
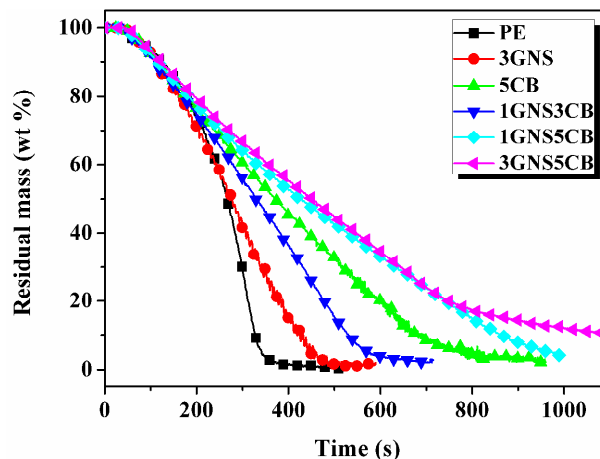


**Fig. 5** Effect of GNS and CB on the normalized mass loss of LLDPE.

**Table 2** Combustion parameters obtained from cone calorimeter tests, LOI tests and vertical burning tests.

| Sample | $t_{ign}$ (s) | PHRR (kW/m$^2$) | THR (MJ/m$^2$) | Residual char [a] (wt %) | LOI value (%) | UL-94 rating |
|--------|------|------|------|------|------|------|
| PE | 61 | 1466 | 193 | 0.4 | 18.0 | N/A [b] |
| 3GNS | 44 | 670 | 193 | 2.0 | 19.2 | N/A |
| 5CB | 51 | 320 | 186 | 2.1 | 25.2 | V2 |
| 1GNS3CB | 45 | 439 | 192 | 2.8 | 25.9 | V2 |
| 1GNS5CB | 45 | 319 | 188 | 4.4 | 26.6 | V2 |
| 3GNS5CB | 48 | 297 | 185 | 10.2 | 27.8 | V2 |

[a] Mass percentage left after testing finished. [b] No rating.

Fig. 4 presents the THR curves for LLDPE and its nanocomposites. Compared to neat LLDPE, the THR of binary nanocomposites (3GNS and 5CB) did not decrease remarkably. Similarly, the THR of ternary LLDPE/GNS/CB nanocomposites was reduced slightly. However, since the slope of THR curve was assumed as representing the fire spread rate,[45] the flame spread of ternary LLDPE/GNS/CB nanocomposites, particularly 3GNS5CB, decreased significantly in comparison with neat LLDPE.

Fig. 5 shows the changes of normalized mass loss of LLDPE and its nanocomposites with combustion time. Addition of GNS alone into LLDPE matrix did not notably decrease the MLR, while adding CB alone into LLDPE matrix led to a dramatic reduction of the MLR in the later stage of combustion. However, the combination of GNS with CB into LLDPE led to a more obvious increase in the residual mass during combustion for more than 500 s compared to binary 5CB nanocomposite. The highest yield of residual char for LLDPE nanocomposites (Table 2) was 10.2 wt % for ternary 3GNS5CB nanocomposite, which was a little higher than the initial total loadings of GNS and CB. This indicated that a part of pyrolytic flammable gases did not quickly volatilize during combustion in the case of ternary 3GNS5CB

nanocomposite.

To further investigate the flame retardancy of LLDPE nanocomposites, LOI and vertical burning tests were carried out. As listed in Table 2, the LOI value increased with the addition of nanofillers, but the increasing amplitude from CB nanoparticles was more significant than that from GNS. The highest value could reach to 27.8 corresponding to ternary 3GNS5CB nanocomposite. However, 3GNS5CB just could pass V2 rating. This is probably because that the contents of GNS and CB in LLDPE are too low to form a protective char layer with high strength to effectively prevent the burning dripping of LLDPE. Further investigations about the improvements of the structure and strength of char layer are being conducted in our laboratory. Nevertheless, the combination of GNS with CB notably promoted the flame retardancy of LLDPE.

### 3.3 Char structure analysis

To analzye the combination of GNS with CB on improving the flame retardancy of LLDPE, the structure of the residual chars after cone calorimeter tests were analyzed. Fig. 6 presents the photographs of the residual chars from LLDPE and its nanocomposites. There was no any char left for neat LLDPE after cone calorimeter test (Fig. 6a). As for binary 3GNS nanocomposite, some block-like gray products were left, which was not continuous (Fig. 6b). Similarly, a few black solids were produced from binary 5CB nanocomposite, and the char layer was not continuous (Fig. 6c). However, a better carbon protective layer from ternary LLDPE/GNS/CB nanocomposites was formed with the combination of GNS and CB, compared to that from binary nanocomposites (3GNS and 5CB). As shown in Figs. 6d and 6e for ternary nanocomposites (1GNS3CB and 1GNS5CB), the char layer gradually became dense, thick and fully covered. Ternary 3GNS5CB nanocomposite exhibited the best carbon protective layer (an integrated and continuous char layer, which was thick and compact) among all the LLDPE nanocomposites (Fig. 6f). Previous report showed that the homogeneity of the residual char was closely related to the PHRR of polymer nanocomposites.[46] The more homogenous the residual chars found, the lower PHRR. Hence, it corresponded to the best flame retardancy.
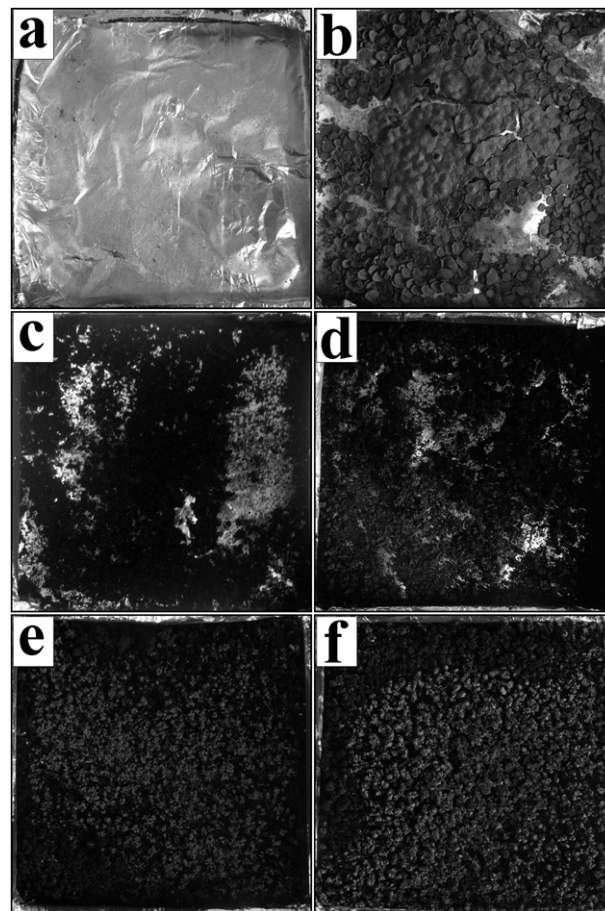


**Fig. 6** Photographs of the residual chars after cone calorimeter tests: (a) neat LLDPE, (b) 3GNS, (c) 5CB, (d) 1GNS3CB, (e) 1GNS5CB and (f) 3GNS5CB.

The interior structure of residual chars from the cone calorimeter tests was further observed by FE-SEM (Fig. 7). As shown in Fig. 7a, the residual char of binary 3GNS nanocomposite consisted of loose GNS, and the cracks and holes throughout the entire residue allowed the escape of pyrolysis gases. The residual char from binary 5CB nanocomposite was aggregate of carbon spheres, which were composed of CB nanoparticles (Fig. 7b and the insetting image). Likewise, a lot of aggregated carbon spheres were observed in the residual chars from ternary LLDPE/GNS/CB nanocomposites (Figs. 7c–7f), and interestingly, GNS was found to be uniformly embedded in the residual chars and closely contacted to aggregated carbon spheres (Fig. 7f). As a result, the residual chars became thicker and more compact.

Hence, the combination of GNS with CB favored the formation of a better dense and continuous carbon protective layer than GNS or CB alone. The improved carbon protective layer displayed two effects at least during the degradation and combustion processes of LLDPE. On one hand, the carbon layer could enhance the physical barrier effect, which not only prevented the diffusion of oxygen into LLDPE matrix, but also hindered the diffusion of volatile decomposition products out of LLDPE. On the other hand, the carbon layer acted as a thermal shield for energy feedback from the flame during combustion.
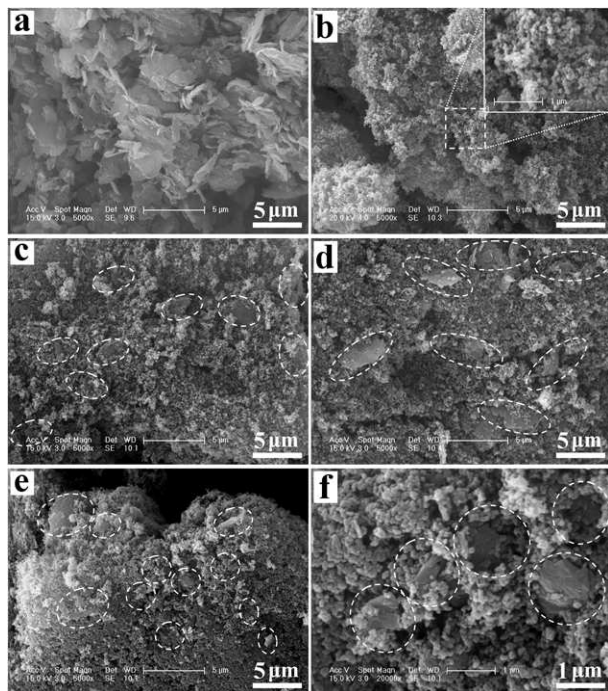
**Fig. 7** Typical FE-SEM images of the residual chars after cone calorimeter tests: (a) 3GNS, (b) 5CB, (c) 1GNS3CB, (d) 1GNS5CB, and (e and f) 3GNS5CB. The inset image (in b) showed the magnification of
5 the marked region, and the region cycled by dashed-line showing the GNS being embedded in the aggregates of carbon spheres (composed of CB nanoparticles).

### 3.3 Mechanism of flame retardancy

Based on the above results, the combination of GNS with CB
10 facilitated the formation of a better dense carbon layer and the improvement of flame retardancy of LLDPE. There are three possible reasons: (i) Physical effect of the combined GNS/CB, that is to say, the formation of a percolated network structure in LLDPE matrix, (ii) the chemical effect of the combined GNS/CB,
15 and (iii) the combination of physical effect and chemical effect.
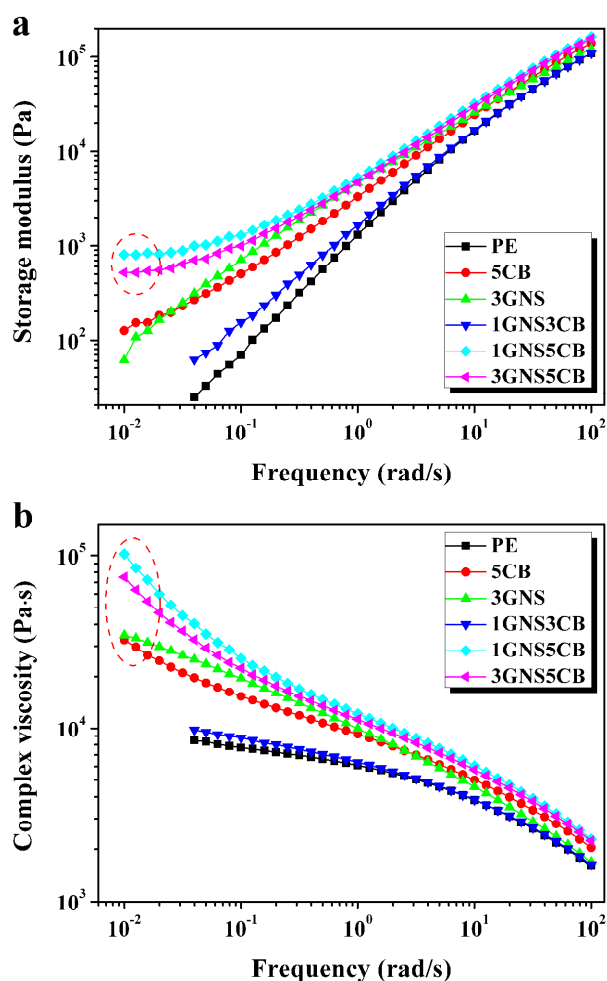


**Fig. 8** Effect of GNS and CB on linear viscoelastic properties: Storage modulus (a) and complex viscosity (b).

For polymer nanocomposites containing nanoparticles, a so-
20 called three-dimensional filler network structure will be formed when the concentration of nanoparticles reaches a threshold value.[14] The formation of a network structure tends to increase the mechanical integrity of a protective layer.[13] To study whether the combination of GNS with CB favor for the formation of a
25 percolated network structure in LLDPE matrix, melt rheological properties of LLDPE and its nanocomposites were investigated. Fig. 8a shows the variations of storage modulus ($G'$) and complex viscosity ($\eta$) as a function of frequency ($\omega$) for LLDPE and its nanocomposites at 160 °C under nitrogen atmosphere. Neat
30 LLDPE exhibited a typical linear polymer-like terminal behavior with scaling properties of approximately $G' \sim \omega^2$, indicating that LLDPE molecular chains were fully relaxed at low frequencies. When GNS (3 wt %) or CB (5 wt %) alone, or the combination of GNS (1 wt %) and CB (3 wt %) was added into LLDPE matrix,
35 there was no plateau at the low frequencies, implying that the concentrations of GNS and CB did not reach the threshold values to form the network. However, the terminal behavior of LLDPE was significantly changed when the concentrations of GNS and/or CB in LLDPE matrix were increased, and the dependence
40 of $G'$ on $\omega$ at low frequency gradually became weak. For ternary nanocomposites (1GNS5CB and 3GNS5CB), the $G'$ curves exhibited distinct plateaus at the low frequencies, which was

similar to the phenomena observed in the poly(methyl methacrylate)/CNT,[6] polystyrene/CNT and polystyrene/clay,[14] and PP/CNT[47] nanocomposites. The above results indicated a transition from liquid-like to solid-like viscoelastic behavior in the ternary nanocomposites (1GNS5CB and 3GNS5CB).

Generally, the melting process and degradation will take place before a material starts to combust, and combustible gas products (degradation products) will traverse from the decomposition zone to the flame zone to maintain combustion. If the melt viscosity is high, the gas products need more time to reach the flame zone, and the combustion process thus will be slowed down. Correspondingly, the changes of $\eta$ for LLDPE and its nanocomposites are shown in Fig. 8b. Neat LLDPE displayed a pseudo-Newtonian behavior at low frequency range, and this behavior did not change significantly with the addition of GNS or CB. Interestingly, in the ternary LLDPE/GNS/CB nanocomposites, especially for 3GNS5CB, a much higher complex viscosity and a pronounced shear thinning behavior were present. This behavior further demonstrated that the combination of GNS with CB played an important role in promoting the formation of percolated network, which was essential to improve the char layer and the flame retardancy of LLDPE.
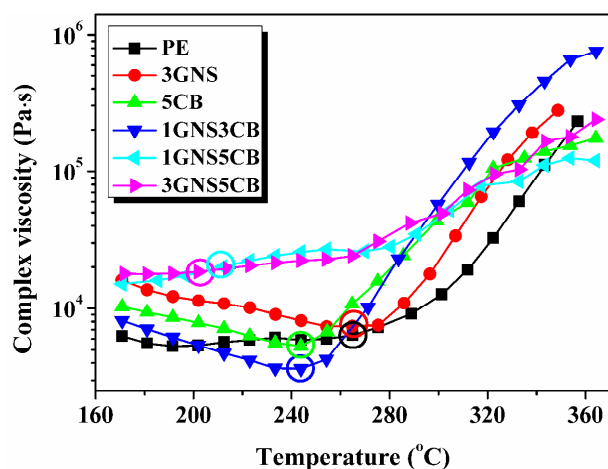


**Fig. 9** Dependence of complex viscosity on temperature for LLDPE and its nanocomposites. The cycled data point displayed the onset temperature for complex viscosity increase of LLDPE and its nanocomposites.

Moreover, during the degradation of LLDPE, the crosslinking of LLDPE radicals will occur, and both the degradation and crosslinking will speed up in the presence of $O_2$. CB was speculated to catalyze the thermal-oxidative crosslinking degradation reaction of LLDPE, which made a positive contribution to the thermal stability and flame retardancy. To confirm this speculation, dynamic temperature scanning measurements were performed on the LLDPE and its nanocomposites under air atmosphere. Fig. 9 presents the curves of temperature dependence of complex viscosity for LLDPE and its nanocomposites. Clearly, all samples first showed a decrease in the complex viscosity with the increase of temperature, followed by a subsequent sharp increase. This was because, upon heating, the easier movement of LLDPE chains and the

degradation at high temperature resulted in a decrease in complex viscosity of the samples. Afterwards, the crosslinking of LLDPE radicals could increase the complex viscosity. However, the onset temperatures for complex viscosity increase of LLDPE nanocomposites were different. For neat LLDPE and binary 3GNS nanocomposite, the temperature at which the complex viscosity began to increase was around 265 °C, while those for binary 5CB and ternary 1GNS3CB nanocomposites decreased down to about 255 °C.

As well known, the polycondensed aromatic rings of CB acts as a strong radical trapping agent.[18] The decreased onset temperature for complex viscosity increase of LLDPE nanocomposites was explained that CB nanoparticles acted as oxidation crosslinking sites to catalyze the oxidation crosslinking reaction of LLDPE chains, which resulted from the reaction between the radicals on the surface of CB and the double bond of the degradation products of LLDPE. This was dominant to influence the viscosity in comparison with the decomposition of LLDPE chains. Strikingly, there were no obvious onset temperatures for complex viscosity increase of ternary 1Si5CB and 3Si5CB nanocomposites, which were roughly estimated to be 244 °C and 223 °C, respectively, lower than that of binary 3GNS or 5CB nanocomposite, or ternary 1Si3CB nanocomposite. Thereby, the combination of GNS with CB was more efficient in catalyzing oxidation crosslinking reaction of LLDPE radicals.
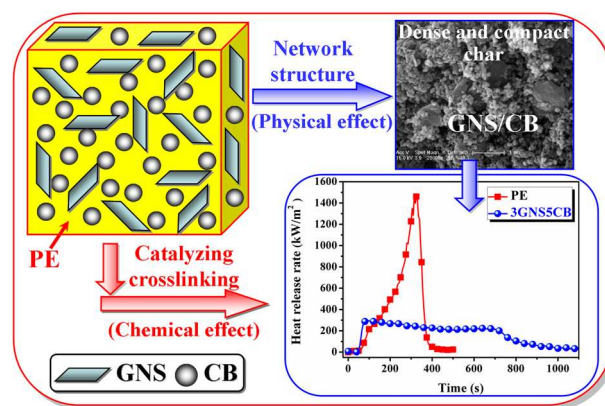


**Fig. 10** Mechanism about the combination of GNS with CB on improving the flame retardancy of LLDPE.

According to the above results, a schematic drawing for the mechanism about the combination of GNS and CB on improving the flame retardancy of LLDPE is shown in Fig. 10. In the combination of GNS with CB, on one hand, a percolated network structure of GNS and CB in LLDPE matrix was formed, which facilitated the formation of a better dense and continuous carbon protective layer during combustion. This not only prevented the diffusion of oxygen into LLDPE matrix, and hindered the diffusion of volatile decomposition products out of LLDPE, but also acted as a thermal shield for energy feedback from the flame. On the other hand, GNS contributed to the oxidation crosslinking reaction of LLDPE radicals catalyzed by CB. Hence, the combination of GNS and CB was displayed on improving the flame retardancy of LLDPE.

## 3.6. Mechanical properties

Clearly, a non-halogen method for improving flame retardancy of polymeric materials along with improving mechanical properties simultaneously is very attractive to academic and industrial communities. The representative stress-strain curves of LLDPE and its nanocomposites are shown in Fig. 11, and the detailed mechanical properties are displayed in Fig. 12. In comparison with neat LLDPE, the yield strength (YS) of binary LLDPE/GNS and 5CB nanocomposites was increased slightly by 6%–15% and 15%, respectively (Fig. 12a). However, the YS of ternary 3GNS5CB nanocomposite was obviously improved from 9.4 to 11.9 MPa by 27%. The tensile strength at break (TSB) of binary 1GNS and 3GNS nanocomposites showed a moderate increase of 21% and 11% (Fig. 12b), respectively, close to that of binary 5CB nanocomposite (11%). Nevertheless, the TSB of ternary LLDPE/GNS/CB nanocomposites was still 11%–18% higher than that of neat LLDPE.
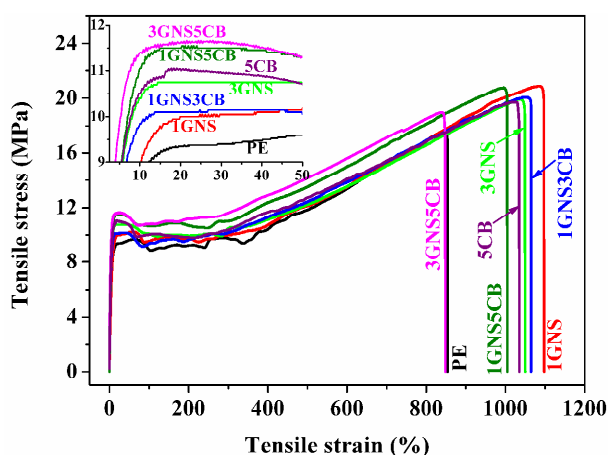


**Fig. 11** Tensile stress-strain curves of LLDPE and its nanocomposites (inset: magnified stress-strain curve in the region of low tensile strain).

Additionally, the elongation at break (EB) of neat LLDPE was improved by 33% and 18%, respectively, after adding 1 wt % or 3 wt % GNS (Fig. 12c), while the addition of 5 wt % CB increased EB somewhat (18%). The incorporation of both GNS and CB improved the EB of LLDPE by 18%–22%, while the EB did not show obvious changes with the incorporation of 3 wt % GNS and 5 wt % CB. This was probably because the more addition amount of GNS and CB inevitably led to the formation of more stress concentration sites, resulting in a weakening effect for the reinforcement of composite materials. The Young's moduli of LLDPE and its nanocomposites are shown in Fig. 12d. On the whole, the Young's moduli of LLDPE nanocomposites were much higher than that of neat LLDPE. The incorporation of 3 wt % GNS and 5 wt % CB alone could enhance the Young's modulus of LLDPE by 111% and 118%, respectively. Although both GNS and CB were commercial and used without any pre-treatments, the ternary LLDPE/GNS/CB nanocomposites showed remarkably higher (90%–219%) Young's moduli than neat LLDPE. This could be attributed to the improvement of the dispersed degrees of both the nanofillers in LLDPE matrix along with good interfacial interactions between the nanofillers and LLDPE matrix.
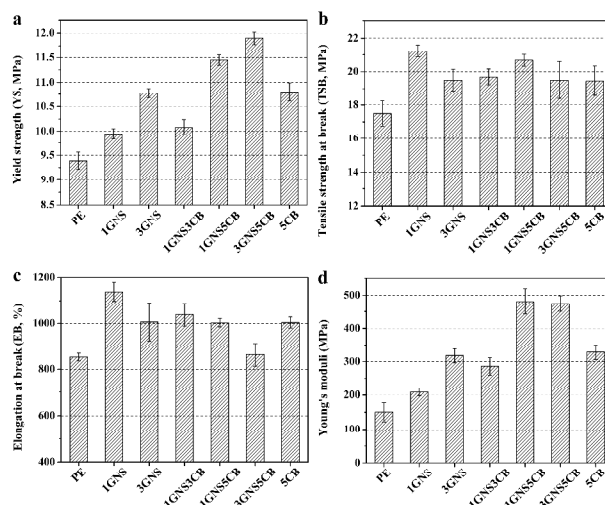


**Fig. 12** Comparison of yield strength (YS, a), tensile strength at break (TSB, b), elongation at break (EB, c), and Young's moduli (d) of LLDPE and its nanocomposites.

## Conclusions

We demonstrated the combination of GNS and CB on simultaneously improving the thermal stability, flame retardancy and mechanical properties of LLDPE. The dramatically improved thermal stability and flame retardancy were partially attributed to the formation of a percolated network structure by GNS and CB in the matrix, and partially to the accelerated oxidation crosslinking reaction of LLDPE radicals catalyzed by GNS and CB. Compared to binary LLDPE/GNS and LLDPE/CB nanocomposites, the percolated network structure of GNS and CB in ternary LLDPE/GNS/CB nanocomposites facilitated the formation of a better dense and continuous carbon protective layer during combustion. This not only prevented the diffusion of oxygen into LLDPE matrix and hindered the diffusion of volatile decomposition products out of LLDPE, but also acted as a thermal shield for energy feedback from the flame. On the other hand, GNS contributed to the oxidation crosslinking reaction of LLDPE radicals catalyzed by CB. Meanwhile, although both GNS and CB were commercial and used without any pre-treatments, both GNS and CB could be well dispersed in LLDPE matrix. The ternary LLDPE/GNS/CB nanocomposites showed much higher mechanical properties compared to neat LLDPE, which was ascribed to their good dispersions and strong interfacial interactions with LLDPE matrix.

## Acknowledgements

## Notes and references

[a] State Key Laboratory of Polymer Physics and Chemistry, Changchun Institute of Applied Chemistry, Chinese Academy of Sciences, Changchun 130022, China. Fax: +86 (0) 431 85262827; Tel: +86 (0) 431 85262004; E-mail: ttang@ciac.ac.cn
[b] University of Chinese Academy of Sciences, Beijing 100049, China

*c Institute of Chemical and Environment Engineering, West Pomeranian University of Technology, Szczecinul. Pulaskiego 10, 70-322 Szczecin, Poland*

## References

1   K. Q. Zhou, W. Yang, G. Tang, B. B. Wang, S. H. Jiang, Y. Hu and Z. Gui, *RSC Adv.*, 2013, **3**, 25030.

2   S. Bourbigot and S. Duquesne, *J. Mater. Chem.*, 2007, **17**, 2283.

3   S. Bourbigot and G. Fontaine, *Polym. Chem.*, 2010, **1**, 1413.

4   Y. B. Luo, X. L. Wang and Y. Z. Wang, *Polym. Degrad. Stab.*, 2012, **97**, 721.

5   J. W. Gilman, C. L. Jackson, A. B. Morgan, R. H. Harris, E. Manias, E. P. Giannelis, M. Wuthernow, D. Hilton and S. H. Phillips, *Chem. Mater.*, 2000, **12**, 1866.

6   T. Kashiwagi, F. M. Du, J. F. Douglas, K. I. Winey, Jr, R. H. Harris and J. R. Shields, *Nat. Mater.*, 2005, **4**, 928.

7   S. S. Rahatekar, M. Zammarano, S. Matko, K. K. Koziol, A. H. Windle, M. Nyden, T. Kashiwagi and J. W. Gilman, *Polym. Degrad. Stab.*, 2010, **95**, 870.

8   S. Bourbigot, D. L. Vanderhart, J. W. Gilman, S. Bellayer, H. Stretz and D. R. Paul, *Polymer*, 2004, **45**, 7627.

9   C. Deng, J. Zhao, C. L. Deng, Q. Lv, L. Chen and Y. Z. Wang, *Polym. Degrad. Stab.*, 2014, **103**, 1.

10   X. L. Wang, Y. Li, B. Li and Y. Z. Wang, *J. Appl. Polym. Sci.*, 2012, **125**, 3463.

11   B. Dittrich, K. A. Wartig, D. Hofmann, R. Mülhaupt and B. Schartel, *Polym. Degrad. Stab.*, 2013, **98**, 1495.

12   Z. H. Tang, Q. Y. Wei, T. F. Lin, B. C. Guo and D. M. Jia, *RSC Adv.*, 2013, **3**, 17057.

13   T. Kashiwagia, F. M. Du, K. I. Winey, K. M. Groth, J. R. Shields, S. P. Bellayer, H. Kim and J. F. Douglas, *Polymer*, 2005, **46**, 471.

14   T. Kashiwagi, M. Mu, K. Winey, B. Cipriano, S. R. Raghavan, S. Pack, M. Rafailovich, Y. Yang, E. Grulke and J. Shields, et al., *Polymer*, 2008, **49**, 4358.

15   S. Bourbigot, G. Fontaine, A. Gallos and S. Bellayer, *Polym. Adv. Technol.*, 2011, **22**, 30.

16   B. Schartel, P. Pötschke, U. Knoll and M. Abdel-Goa, *Eur. Polym. J.*, 2005, **41**, 1061.

17   P. A. Song, Y. Zhu, L. F. Tong and Z. P. Fang, *Nanotechnology*, 2008, **19**, 225707.

18   X. Wen, Y. J. Wang, J. Gong, J. Liu, N. N. Tian, Y. H. Wang, Z. W. Jiang, J. Qiu and T. Tang, *Polym. Degrad. Stab.*, 2012, **97**, 793.

19   S. Liu, H. Q. Yan, Z. P. Fang, Z. H. Guo and H. Wang, *RSC Adv.*, 2014, **4**, 18652.

20   P. A. Song, Y. Shen, B. Du, Z. H. Guo and Z. P. Fang, *Nanoscale*, 2009, **1**, 118.

21   P. A. Song, L. N. Liu, S. Y. Fu, Y. M. Yu, C. D. Jin, Q. Wu, Y. Zhang and Q. Li, *Nanotechnology*, 2013, **24**, 125704.

22   K. Fukushima, M. Murariu, G. Camino and P. Dubois, *Polym. Degrad. Stab.*, 2010, **95**, 1063.

23   F. Gao, G. Beyer and Q. Yuan, *Polym. Degrad. Stab.*, 2005, **89**, 559.

24   W. D. Zhang, I. Y. Phang and T. X. Liu, *Adv. Mater.*, 2006, **18**, 73.

25   C. Zhang, W. W. Tjiu, T. X. Liu, W. Y. Lui, I. Y. Phang and W. D. Zhang, *J. Phys. Chem. B*, 2011, **115(13)**, 3392.

26   Z. Wang, X. Y. Meng, J. Z. Li, X. H. Du, S. Y. Li, Z. W. Jiang and T. Tang, *J. Phys. Chem. C*, 2009, **113**, 8058.

27   H. Y. Ma, L. F. Tong, Z. B. Xu and Z. P. Fang, *Nanotechnology*, 2007, **18**, 375602.

28   P. A. Song, L. P. Zhao, Z. H. Cao and Z. P. Fang, *J. Mater. Chem.*, 2011, **21**, 7782.

29   M. K. Liu, C. Zhang, W. W. Tjiu, Z. Yang, W. Z. Wang and T. X. Liu, *Polymer*, 2013, **54**, 3124.

30   T. Tang, X. C. Chen, X. Y. Meng, H. Chen and Y. P. Ding, *Angew. Chem. Int. Ed.*, 2005, **44**, 1517.

31   T. Tang, X. C. Chen, H. Chen, X. Y. Meng, Z. W. Jiang and W. G. Bi, *Chem. Mater.*, 2005, **17**, 2799.

32   R. J. Song, Z. W. Jiang, H. O. Yu, J. Liu, Z. J. Zhang, Q. W. Wang and T. Tang, *Macromol. Rapid. Commun.*, 2008, **29**, 789.

33   H. O. Yu, Z. W. Jiang, J. W. Gilman, T. Kashiwagi, J. Liu, R. J. Song and T. Tang, *Polymer*, 2009, **50**, 6252.

34   H. O. Yu, Z. J. Zhang, Z. Wang, Z. W. Jiang, J. Liu, L. Wang, D. Wan and T. Tang, *J. Phys. Chem. C*, 2010, **114**, 13226.

35   H. O. Yu, J. Liu, Z. Wang, Z. W. Jiang and T. Tang, *J. Phys. Chem. C*, 2009, **113**, 13092.

36   X. Wen, J. Gong, H. O. Yu, Z. Liu, D. Wan, J. Liu, Z. W. Jiang and T. Tang, *J. Mater. Chem.*, 2012, **22**, 19974.

37   J. Gong, N. N. Tian, J. Liu, K. Yao, Z. W. Jiang, X. C. Chen, X. Wen, E. Mijowska and T. Tang, *Polym. Degrad. Stab.*, 2014, **99**, 18.

38   J. Gong, N. N. Tian, X. Wen, X. C. Chen, J. Liu, Z. W. Jiang, E. Mijowska and T. Tang, *Polym. Degrad. Stab.*, 2014, **104**, 18.

39   T. Kuilla, S. Bhadra, D. Yao, N. H. Kim, S. Bose and J. H. Lee, *Prog. Polym. Sci.*, 2010, **35**, 1350.

40   B. Hu, K. Wang, L. H. Wu, S. H. Yu, M. Antonietti and M. M. Titirici, *Adv. Mater.*, 2010, **22**, 813.

41   "What is Carbon Black". International Carbon Black Association. Retrieved 2009-04-14. http://www.carbon-black.org/index.php/what-is-carbon-black.

42   X. Wen, N. N. Tian, J. Gong, Q. Chen, Y. L. Qi, Z. Liu, J. Liu, Z. W. Jiang, X. C. Chen and T. Tang, *Polym. Adv. Technol.*, 2013, **24**, 971.

43   J. Gong, R. Niu, N. N. Tian, X. C. Chen, X. Wen, J. Liu, Z. Y. Sun, E. Mijowska and T. Tang, *Polymer*, 2014, **55(13)**, 2998.

44   J. D. Peterson, S. Vyazovkin and C. A. Wight, *Macromol. Chem. Phys.*, 2001, **202(6)**, 775.

45   N. N. Tian, J. Gong, X. Wen, K. Yao and T. Tang, *RSC Adv.*, 2014, **4**, 17607.

46   M. Bartholmai and B. Schartel, *Polym. Adv. Technol.*, 2004, **15**, 355.

47   S. B. Kharchenko, J. F. Douglas, J. Obrzut, E. A. Grulke and K. B. Migler, *Nat. Mater.*, 2004, **3(8)**, 564.

**Table of Contents (TOC)**

# Simultaneously improving the thermal stability, flame retardancy and mechanical properties of polyethylene by the combination of graphene with carbon black

5 **Jiang Gong, Ran Niu, Jie Liu, Xuecheng Chen, Xin Wen, Ewa Mijowska, Zhaoyan Sun and Tao Tang***

A novel combination of GNS with CB was demonstrated to improve thermal stability, flame retardancy and mechanical properties of LLDPE.

10